ELSEVIER

Coastal Engineering 29 (1996) 47–78

COASTAL ENGINEERING

The growth of fetch limited waves in water of finite depth. Part 1. Total energy and peak frequency

I.R. Young [a], L.A. Verhagen [b]

[a] *School of Civil Engineering, University College, Univ. of N.S.W., Canberra, A.C.T. 2600, Australia*
[b] *HASKONING, P.O. Box 151, 6500 AD Nijmegen, Netherlands*

Received 17 August 1995; accepted 9 February 1996

Abstract

The results of a fetch limited wind wave growth experiment in water of finite depth are presented. The experiment involved measurements of wind wave spectra, wind speed and direction at eight stations along the fetch. The site for the experiment was a lake with an almost constant water depth of 2 m. The results clearly show the evolution of both the non-dimensional total energy and peak frequency as a function of non-dimensional fetch. At short fetch, the waves are in deep water and the results are comparable to previous deep water measurements. As the fetch increases, the results diverge from the deep water case. Both the growth of total energy and the migration of the peak frequency to lower values are reduced in comparison to results from deep water conditions. At large fetch, evolution of both total energy and peak frequency ceases, both parameters becoming depth limited. Rather than there being a single growth law formula, as in deep water, a family of curves are developed, one for each value of non-dimensional depth.

1. Introduction

Commencing with the cornerstone JONSWAP experiment (Hasselmann et al., 1973), the investigation of the evolution of deep water wind generated ocean waves has been a common theme. Although this case represents a very idealized situation, the resulting evolution provides valuable insight into the complex physics of wind wave evolution. In addition, the resulting non-dimensional growth curves have proved a valuable aid to preliminary engineering design and for use in the validation of comprehensive spectral models.

The limitation of such studies to deep water is restrictive, particularly when it is considered that a significant percentage of coastal engineering works are in areas where finite water depth will influence the resulting wave field. Despite the obvious require-

0378-3839/96/$15.00 Published by Elsevier Science B.V.
PII S0378-3839(96)00006-3

ment, there exists no comprehensive counterpart to JONSWAP (Hasselmann et al., 1973) in finite depth water.

This paper presents the results of such an experiment. The evolution of the wave spectrum has been measured at a number of points along a shallow lake. The relatively simple geometry and bathymetry of the lake and the absence of contaminating swell results in a near ideal test basin in which to investigate fetch limited growth in finite depth water.

The arrangement of the paper is as follows. Section 2 presents a review of existing knowledge of finite depth fetch limited growth. This is followed in Section 3 by a comprehensive description of the measurement basin and experimental design. Section 4 describes the instrumentation and data reduction and analysis techniques adopted. An overview of the extensive data set is provided in Section 5. The results of the experiment will be presented in terms of non-dimensional variables and Section 6 discusses the appropriate values of wind speed and water depth to be used in these variables. Section 7 presents results from the experiment which confirm the existence of an asymptotic depth limit to growth. This result is extended in Section 8 to develop non-dimensional growth curves which are a function of both non-dimensional depth and fetch. A comprehensive error analysis and the potential consequences for the experimentally derived results are presented in Section 9, followed by conclusions in Section 10. Finally, a second part to this paper is foreshadowed, in which the detailed evolution of the full spectral shape will be discussed. The present paper is confined to discussion of the summary spectral parameters of total energy and peak spectral frequency.

2. Previous studies of fetch limited growth

The first comprehensive study of fetch limited growth in deep water was that of JONSWAP (Hasselmann et al., 1973). To this day, it remains one of the very few *true* fetch limited studies, in that multiple stations were located at varying fetches. The majority of subsequent studies, such as those of Kahma (1981) and Donelan et al. (1985, 1992), have considered data from a single location. In such situations, variation in the non-dimensional fetch can be introduced through consideration of cases of varying wind speed. Multiple fetch, deep water studies include those of Donelan et al. (1992) and Dobson et al. (1989) which used conventional insitu instruments. Remote sensing techniques have also been used to investigate the fetch limited development of significant wave height (Walsh et al., 1989; Ebuchi et al., 1992).

The composite data set from the various deep water studies is extensive and there is clear evidence that the data can be represented in terms of relatively simple non-dimensional variables: non-dimensional energy, $\epsilon = g^2E/u^4$, non-dimensional frequency, $\nu = f_p u/g$ and non-dimensional fetch $\chi = gx/u^2$, where g is gravitational acceleration, E is the total wave energy or variance of the wave record, f_p is the frequency of the spectral peak and u is a characteristic wind velocity (see Section 6). Despite these relatively simple non-dimensional groupings, there appear to be inconsistencies between the various data sets and scatter within individual data sets. Attempts to explain these discrepancies (Battjes et al., 1987; Kahma and Calkoen, 1992) have been insightful, but questions about the appropriate scaling of such experimental data still exists.

In comparison to the deep water case, the available data for fetch limited growth in finite depth situations is very limited. The first study of shallow water wave growth was conducted by Thijsse (1949). This was followed by the field investigations staged in Lake Okeechobe, USA (U.S. Army Corps of Engineers, 1955; Bretschneider, 1958). This experiment was limited by available instrumentation of the time (paper tape recording) and was largely concentrated on determining the depth limited asymptotes to growth, rather than defining evolution with fetch. Using these data, Bretschneider (1958) adopted the wind velocity measured at a reference height of 10 m, U_{10} as the appropriate scaling parameter for wind speed and determined asymptotic limits to the development of non-dimensional energy and frequency. These limits can be represented as (CERC, 1977)

$$\epsilon = 1.4 \times 10^{-3} \delta^{1.5} \tag{1}$$

$$\nu = 0.16 \delta^{-0.375} \tag{2}$$

where $\epsilon = g^2 E / U_{10}^4$, $\nu = f_p U_{10} / g$, $\delta = gd/U_{10}^2$ and d is the water depth.

Ijima and Tang (1966) combined the results of Eqs. (1) and (2) with available deep water fetch limited results and numerical modelling of the effects of bottom friction and percolation (Bretschneider and Reid, 1953) to develop a set of fetch limited finite depth growth curves for ϵ and ν. These results appeared in CERC (1977). They were further revised in CERC (1984) to be consistent with the JONSWAP (Hasselmann et al., 1973) deep water results, appearing as

$$\epsilon = 5 \times 10^{-3} \left\{ \tanh A_1 \tanh \left[\frac{B_1}{\tanh A_1} \right] \right\}^2 \tag{3}$$

where

$$A_1 = 0.53 \delta^{0.75} \tag{4}$$

$$B_1 = 5.65 \times 10^{-3} \chi^{0.5} \tag{5}$$

and

$$\nu = 0.133 \left\{ \tanh A_2 \tanh \left[\frac{B_2}{\tanh A_2} \right] \right\}^{-1} \tag{6}$$

where

$$A_2 = 0.833 \delta^{0.375} \tag{7}$$

$$B_2 = 3.79 \times 10^{-2} \chi^{0.33} \tag{8}$$

and $\chi = gx/U_{10}^2$.

Eqs. (3) and (6) reduce to the experimentally confirmed forms Eqs. (1) and (2) for the asymptotic limit of small d and large x and to the JONSWAP (Hasselmann et al., 1973) results for the limits of large d and small x. The form of the relationship between these limits relies completely on the results of the numerical modelling of Ijima and Tang (1966), without any experimental corroboration.

Bouws (1986) reported the results from single point measurements in shallow (≈ 4 m) Lake Marken, The Netherlands. As there was only one experimental site, there was little variation in the fetch x. Due to the similarity of the non-dimensional scaling for $\chi = gx/u^2$ and $\delta = gd/u^2$, small δ is always associated with small χ and large δ with large χ. Hence, confirmation of results such as (3) and (6) becomes difficult. The introduction of the additional non-dimensional variable, δ strengthens the requirements for multiple fetch measurements. Nevertheless, Bouws (1986) confirmed that the growth rate for ϵ as a function of χ was less than that reported from deep water experiments. More surprisingly, the data indicated that the development of ν with χ was comparable to deep water. In addition, Bouws (1986) adopted a non-dimensional scaling in terms of the friction velocity, u_* rather than U_{10}, claiming this reduced scatter in the results.

3. Description of experiment

The ideal site for a fetch limited finite depth wave evolution experiment would consist of a large body of water of shallow and uniform depth with a long straight shoreline. In addition, the site should be free from the contaminating effects of swell and have meteorological conditions such that consistent winds blow perpendicular to the shoreline. Clearly, such ideal conditions never exist, but a reasonable approximation can be found in shallow lakes as utilized in the Lake Okeechobe (U.S. Army Corps of Engineers, 1955; Bretschneider, 1958) and Lake Marken (Bouws, 1986) experiments. The site chosen for the present experiment was Lake George (see Fig. 1). The lake is

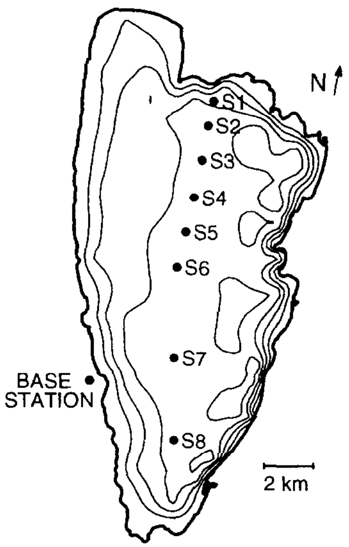

Fig. 1. Map of the Lake George experimental site. The measurement locations are labelled S1 to S8. Data were transmitted to the Base Station on the western shore of the lake where it was logged under computer control. The contour interval is 0.5 m, with the maximum contour value 2 m.

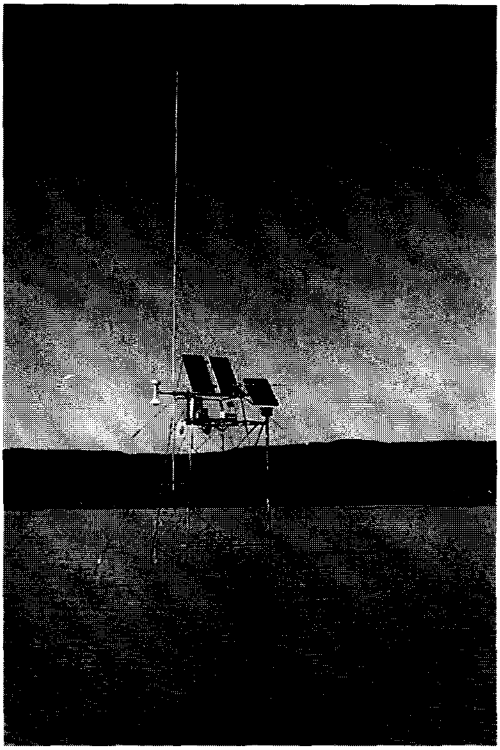

Fig. 2. A photograph of measurement station S8. The Zwarts pole is to the right of the tower. The solar cells used to power the system are clearly visible. The white module to the left is an aspirated radiation shield for the measurement of air temperature and humidity. The telemetry aerial and the anemometer masts are also clearly visible.

approximately 20 km long by 10 km wide and has a relatively uniform bathymetry with an approximate water depth of 2 m. A series of 8 measurement stations were established along the long North–South axis of the lake as shown in Fig. 1. With the exception of Station 6, the sites consisted of minimum blockage space frame towers, designed to provide minimum contamination to either wind or wave measurements made from the towers (see Fig. 2). The central site, Station 6, consisted of a large platform with temporary accommodation for the research team (see Fig. 3). Each of the sites was instrumented with a surface piercing wave gauge (Zwarts pole, see Section 4). In addition, cup anemometers at a reference height of 10 m were located at Stations 2, 4, 6, 7 and 8. Air temperature and relative humidity and water temperature were also measured at Stations 2, 6 and 8. A spatial array consisting of 7 Zwarts poles (Young et al., 1995) was established adjacent to the platform at Station 6 to provide high resolution measurements of the directional wave spectrum. A full summary of the instrumentation and characteristics of the measurement sites are contained in Tables 1 and 2.

Although the full experiment spanned a period of approximately 3 years, the data to be discussed in this paper were collected in the approximately 18 month period between

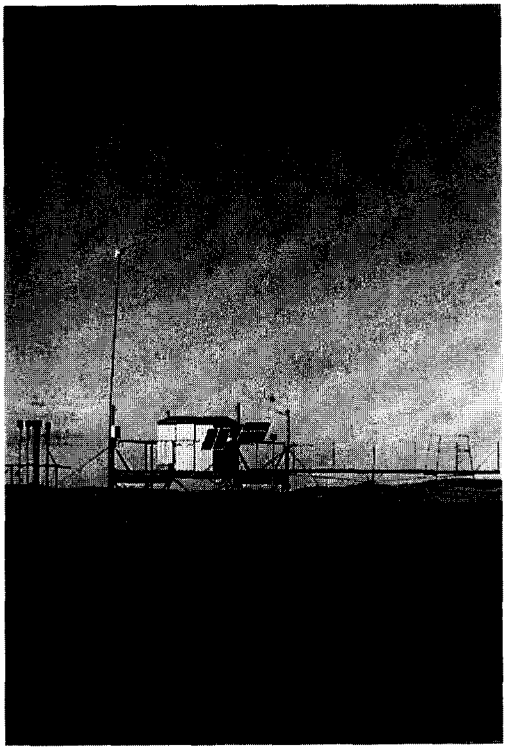

Fig. 3. A photograph of the research platform which was located at station S6. A measurement bridge extends to the right of the main structure. The spatial cluster of wave poles used to measure the directional spectrum is visible to the left of the platform. the anemometer mast, accommodation module and solar panels are also visible.

19 April, 1992 and 3 October, 1993. During this period of time the water depth as measured at Station 5 varied between 1.81 m and 2.00 m.

As shown in Fig. 1, the instrument array is aligned approximately north/south to

Table 1
Characteristics of the measurement sites. The water depth refers to measurements made on 19 April, 1992

Station	Depth (m)	Fetch to North (m)	Fetch to South (m)	Average depth over N fetch (m)	Average depth over S fetch (m)
1	1.68	1,300	15,700	1.09	1.79
2	1.81	2,300	14,700	1.39	1.79
3	1.76	3,700	13,300	1.55	1.79
4	1.79	5,300	11,700	1.62	1.79
5	1.90	6,700	10,300	1.66	1.78
6	1.94	8,100	8,800	1.71	1.77
7	2.04	11,800	5,200	1.80	1.62
8	2.01	15,300	1,700	1.85	0.92

Table 2
Data measured at each of the stations. Quantities marked with ● indicate data measured continuously and transmitted to the base station in real time using telemetry. Quantities marked with * indicate data measured intermittently and stored at the measurement site for later retrieval

Station	Water surface time series	Wind speed and dir.	Air temp., humidity	Water temp.	Directional spectrum
1	●				
2	●	*	*	*	
3	●				
4	●	*			
5	●				
6	●	●	●	●	*
7	●	*			
8	●	*	*	*	

take advantage of the long fetch in this direction and also because the land to the north and south of the lake is relatively flat and free from obstructions. Hence, up-wind influences should introduce no major disturbances to the atmospheric boundary layer flow. As will be detailed in Section 5 and Section 8, the array alignment means that only cases for which the wind direction closely aligns with the north/south direction can be utilized for multi-fetch analysis. This greatly reduces the available data and necessitated the very lengthy experimental period (18 months). This requirement imposed a number of constraints on the experimental design. In particular, the instrumentation needed to be robust and require little maintenance over long periods of time. In addition, the bulk of the data needed to be transmitted to shore using telemetry. This reduced the need for regular maintenance visits and provided real time monitoring of instrument performance.

The primary water surface elevation instrumentation consisted of surface piercing Zwarts poles (Zwarts, 1974; see Section 4). These instruments measure both the mean water depth and the fluctuating water surface elevation, require no regular calibration and significantly less maintenance than alternatives such as capacitance or resistance wires. Data from the Zwarts poles were digitized at a rate of 8 Hz and transmitted in real time via telemetry systems to a base station located on the western shore of the lake. In addition, meteorological information was transmitted in real time from Station 6 at a rate of 1 Hz. Data acquisition and storage was achieved at the base station using a PC based logging system. The logging cycle consisted of a 30 minute logging period, commencing at the start of each hour. The remaining 30 minute period each hour was available for data storage and checking of instrument performance. The logging continued 24 hours per day. A telephone modem link was established between the base station and our laboratory in Canberra, thus enabling regular monitoring of experimental performance. The base station was visited once per week and the data down loaded to a portable PC. At the logging rates indicated above, approximately 100 Mbytes of data were acquired per week.

Meteorological data from stations other than Station 6 were recorded in the form of 10 minute mean values and stored on site using data loggers (see Table 2). These data were down loaded approximately once per month during maintenance visits.

In addition to the instrumentation described above, a spatial array of seven Zwarts poles was located adjacent to the research platform at Station 6. Logging of this instrumentation was controlled by a PC located on the platform. This computer could be operated remotely from our laboratory using a combination of telephone and radio modem links. Data were recorded intermittently, whenever conditions appeared appropriate. In addition, a limited number of measurements of atmospheric turbulence were made using a sonic anemometer during periods when personnel were in attendance at the platform. Neither of these forms of data will be discussed in any detail in this paper.

4. Instrumentation and data processing

As mentioned in Section 3, the primary instrumentation used for the measurement of the water surface elevation were surface piercing Zwarts poles (Young et al., 1995) (also known as transmission line wave gauges). These instruments consist of two concentric aluminium tubes forming the equivalent of a coaxial cable. Water can enter the annulus between the two tubes through a series of holes drilled in the outer tube. The interface between air and water within the annulus represents a sharp discontinuity in the dielectric properties of the coaxial cable, the position of which can be determined with high precision. Provided there is a free passage of water into and out of the annulus, the position of this discontinuity equates to the position of the water surface elevation.

As the peak spectral frequencies of the waves which occur at the short fetches within the lake are relatively high ($f_p \approx 0.25$ to 0.6 Hz), the poles were specifically designed to achieved a high frequency response. Dynamic calibrations of the poles were performed by vertically oscillating the pole in still water at known frequencies. The frequency response of the pole can be increased by progressively increasing the number of holes in the outer tube. Naturally, a point will eventually be reached were a further increase in the porosity of the tube will significantly degrade the structural integrity of the tube. The final system consisted of tubes with outer diameters of 50 mm and 25 mm with an annular gap of 8 mm. In addition to the dynamic calibration performed in still water, insitu comparisons were made against two wire resistance gauges. These intercomparisons showed that the Zwarts poles and resistance wires produced estimates of f_p which were identical at the finite resolution possible within the adopted spectral analysis. In addition, values of E agreed to within 3%. The frequency response of the Zwarts poles declined above $3f_p$. Although this is of significance for the estimate of the detailed spectral shape, it has no consequence for the determination of either f_p or E.

The water surface elevation was digitized at a rate of 8 Hz and transmitted to the base station. Each data point was *tagged* with a sequence count to enable possible transmission errors to be flagged during post-processing. Thirty minute time series of the water surface elevation were recorded for each of the poles, leading to time series of 14,400 points. The time series were sub-divided into 256 point sections and energy spectra determined using ensemble averages of the sub-divided time series. The resulting spectra have 112 degrees of freedom, a Nyquist frequency of 4 Hz and a frequency resolution of 0.031 Hz. The total energy, E was determined from the integral of the spectrum, $F(f)$ and the peak spectral frequency, f_p using the weighted integral (Young, 1996)

$$f_p = \frac{\int f[F(f)]^5 \mathrm{d}f}{\int [F(f)]^5 \mathrm{d}f} \tag{9}$$

A relationship such as Eq. (9) reduces the errors associated with the estimate of f_p from the spectrum which is evaluated only at discrete values of frequency (Young, 1996).

The mean water level at each pole was determined from the means of the 30 minute time series averaged over a 24 hour period. The averaging process removed fluctuations associated with seiching and other long period oscillations within the lake. Such long term fluctuations of the water surface were however relatively minor, never exceeding more than 10 cm in magnitude. The consequences for the resulting errors in the determination of water depth, d and other errors in the analysis will be discussed in detail in Section 9.

As indicated in Table 2, anemometers were located at a reference height of 10 m at Stations 2, 4, 6, 7 and 8. The instrument located at Station 6 was an R.M. Young (Model 05103) anemometer whilst V.D.O. (Model 402 715) instruments were located at the other stations. The analog output from Station 6 was digitized at a rate of 1 Hz and transmitted to the base station in real time via the telemetry system. At all other stations, wind speed and direction were logged and stored in the form of 10 minute means. These data were recovered on monthly maintenance visits. The V.D.O. systems proved relatively unreliable and hence the data record from these instruments is incomplete. A full record, however, exists at Station 6. The data from Station 6 were processed to form 10 minute means which have been used in all subsequent data analysis.

5. Data summary and selection

The full data set collected during the measurement period consisted of approximately 65,000 30-minute time series together with meteorological data from, at a minimum, Station 6. A statistical summary of the data set is contained in Fig. 4. Fig. 4a shows a histogram of the number of observations as a function of wind direction. The full data set is shown. It is clear from this figure, that the predominant wind direction is from the west. Easterly wind directions are also relatively common. These easterly winds are usually associated with the development of afternoon sea breezes during summer. It is also clear that northerly and southerly winds are quite rare. As these were the two wind directions for which the instrument array was optimally designed (see Fig. 1), the need to continue the experiment for an extended period of time (approximately 3 years) to build up an extensive data set becomes clear.

Fig. 4b shows the distribution of wind speed for both the full data set and the north/south data set (shaded). The north/south data set is defined by wind directions

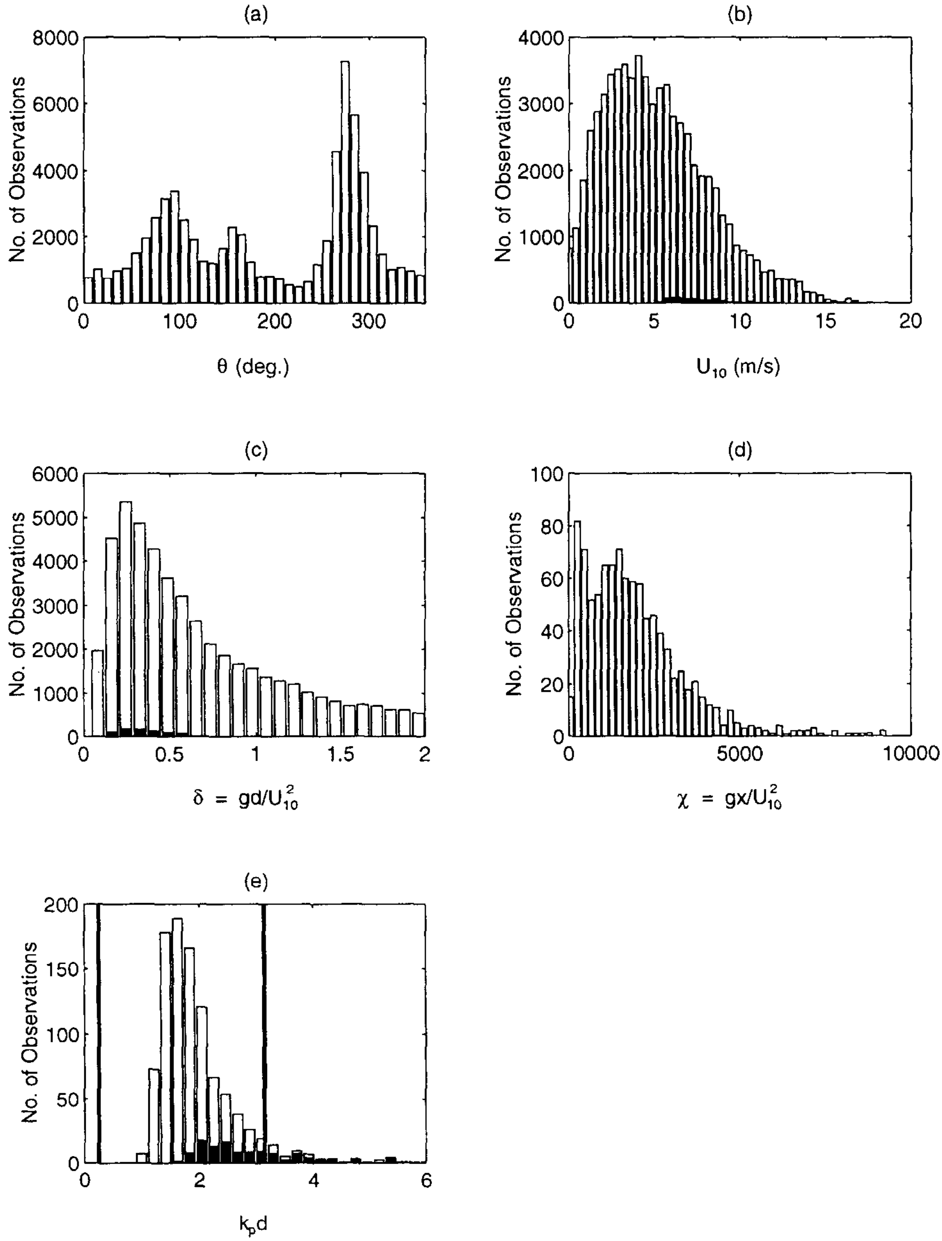

Fig. 4. Summary histograms of data acquired during the experiment. (a) Wind direction for the full data set; (b) Wind speed for the full data set with the north/south data shaded; (c) Non-dimensional water depth, δ for the full data set with the north/south data shaded; (d) Non-dimensional fetch, χ for the north/south data set; (e) The depth parameter, $k_p d$ for the north/south data with data from the first station in the fetch shaded. The vertical lines mark the shallow (left line) and deep (right line) limits.

which are within 20° of the alignment of the instrument array. As can be seen in Fig. 4b, this data set is only a small fraction of the full data set, consisting of approximately 1000 observations. The full data set contains wind speeds up to 20 m/s, with the most common wind speeds in the range 4 to 7 m/s. The maximum wind speed within the north/south data set is 15.2 m/s with the majority of the data within the 5 to 10 m/s band. Only data for which the wind speed and direction were relatively constant during the 30 minute sampling period have been retained in both data sets. The criteria used for this selection were that the wind speed should not vary by more than 10% nor the wind direction by more than 10° during the 30 minute sampling period. Higher winds were observed during the passage of storms across the lake with wind speeds as high as 50 m/s occurring on one brief occasion during the experimental period. A sustained event which occurred after the completion of the experiment produced winds of 35 m/s for a period of 4 hours. This event toppled a number of the towers (uninstrumented at the time) and substantially damaged the platform at Station 6.

The distribution of the non-dimensional water depth, $\delta = gd/U_{10}^2$ is shown for both data sets in Fig. 4c. Both data sets show a peak in the $\delta = 0.2$–0.4 range. For all but the shortest fetch conditions, such waves will be influenced by the bottom. The distribution of non-dimensional fetch $\chi = gx/U_{10}^2$ for the north/south data set is shown in Fig. 4d. Only the north/south data set is shown since, for other directions, the wind is generally at an angle to the shore and a slanting fetch exists. In such cases, the effective fetch is difficult to estimate. In the analysis to follow, however, the extensive east/west data (perpendicular to the long eastern and western shorelines) will also be examined. Fig. 4d shows values of χ ranging from 40 to almost 10,000. This range of χ is almost identical to that covered by the JONSWAP experiment (Hasselmann et al., 1973), indicating that the range of non-dimensional fetch spanned by this data set is extensive.

A clear indication of the potential influence of finite depth on the data is contained in Fig. 4e, which shows the distribution of the quantity $k_p d$, where k_p is the wavenumber of the spectral peak, and d is the water depth. Values of $k_p d > \pi$ are normally considered to represent deep water conditions whilst $k_p d < 0.25$ represents shallow water. These limits are shown on Fig. 4e, the vast majority of the data lying between these values (i.e. in transitional water depth). The data does, however, also extend into the deep water regime, indicating that it should be capable of representing the transition from deep water to regions where bottom influences are significant.

6. Appropriate scaling parameters

The concept that fetch limited growth as described in Section 2 could be represented in terms of the non-dimensional variables ϵ, ν and χ was first proposed by Kitaigorodskii (1962). The method was subsequently shown to have a theoretical justification in terms of the "self-similarity" of the spectrum caused by the shape stabilizing effects of nonlinear interactions within the spectrum (Hasselmann et al., 1973; Young and Van Vledder, 1993). There is however significant debate as to the correct values of wind speed, fetch and water depth (when δ is also included) which should be adopted in these non-dimensional variables. The parameters adopted for the present analysis are discussed below.

6.1. Wind speed

There has been considerable debate as to the appropriate wind speed to use in the non-dimensional variables. These variables are particularly sensitive to the choice of the scaling wind speed, u with $\epsilon \propto u^{-4}$, $\chi \propto u^{-2}$, $\delta \propto u^{-2}$ and $\nu \propto u$. The original Kitaigorodskii similarity law (Kitaigorodskii, 1962) was expressed in terms of U_{∞}, the wind speed at the edge of the atmospheric boundary layer. This value is commonly replaced by a more measurable quantity. Kitaigorodskii (1962) originally suggested the use of the friction velocity u_*, this choice subsequently being supported by Kahma and Calkoen (1992). The two best known deep water fetch limited growth experiments, JONSWAP (Hasselmann et al., 1973) and Lake Ontario, (Donelan et al., 1985) have both used the wind speed measured at a reference height of 10 m, U_{10}. In a compelling argument, Donelan and Pierson (1987) have proposed the use of the wind speed measured at a height of $\lambda/2$, where λ is the wave length. Hence, the reference anemometer height varies with the scale of the waves.

The quantity, U_{10} was measured at multiple stations during this experiment, hence this quantity is directly available. In contrast, u_* and $U_{\lambda/2}$ must be derived from U_{10}. Rather than simply being a function of U_{10} (Charnock, 1955; Wu, 1982), the drag coefficient, C_d is believed to also depend on sea-state, in particular the high frequency tail of the spectrum (Janssen, 1989; Smith et al., 1992). In water of finite depth the spectral shape differs from that in deep water (Bouws et al., 1985). The effect of such differences on C_d and hence u_* is unknown. Similarly, if $U_{\lambda/2}$ is to be adopted, it must be calculated with the aid of an assumed boundary layer profile (logarithmic). Again, such a calculation depends on the surface roughness, (C_d).

Initial investigations were conducted utilizing each of the above parameters as the scaling wind velocity. Both non sea-state and deep water sea-state representations were used for C_d. In all cases, U_{10} produced the minimum scatter in the data. This may not necessarily indicated that it is the most appropriate scaling parameter, merely that the errors introduced in the indirect determinations of u_* and $U_{\lambda/2}$ are substantial. For this reason, U_{10} has been adopted as the wind speed scaling parameter in the present analysis.

One of the primary assumptions in fetch limited growth is that the wind speed is constant over the fetch. Even in the most stable of meteorological conditions, such a situation does not occur. At the shoreline there is a discontinuity in the surface roughness, from the aerodynamically "rough" land surface to the relatively smooth water surface. As a result, an internal marine boundary layer begins to grow within the thicker terrestrial boundary layer. Hence, the wind speed measured at a constant reference height will gradually increase moving down the fetch. The development of such internal boundary layers has been previously investigated by Taylor and Lee (1984) and Smith and MacPherson (1987), and in the context of fetch limited growth by Dobson et al. (1989) and Kahma and Calkoen (1992). Fig. 5 shows three examples of

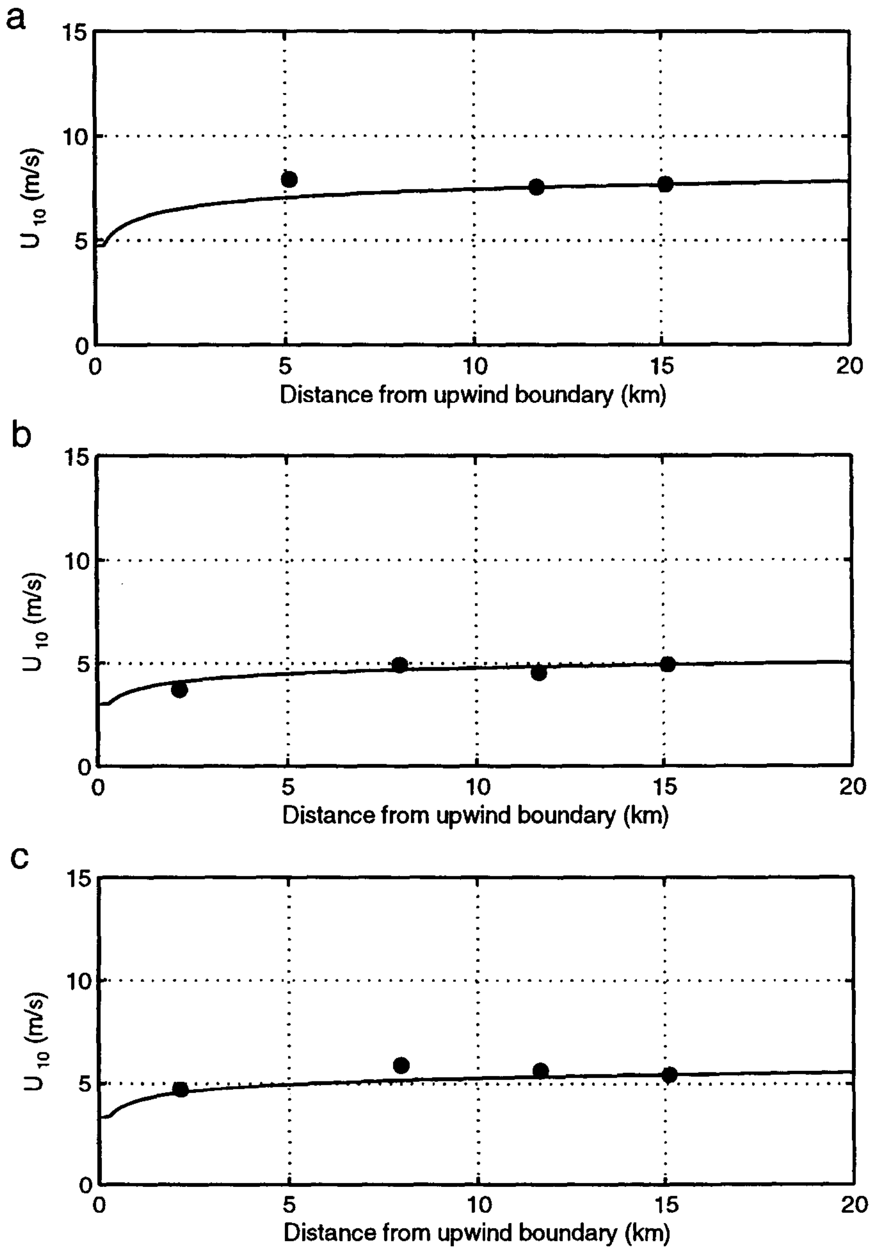

Fig. 5. Three examples of the increase in the wind speed, U_{10} with fetch. Measured data are shown by the points with the model of Taylor and Lee (1984) (Eq. (11)) as the curve. All cases are for northerly winds and z_{0u} was assumed to be 0.5 m.

the variation in wind speed (U_{10}) with fetch as recorded by the anemometers in this experiment.

Taylor and Lee (1984) find that the variation of the wind speed in such cases can be modelled by the assumption that the thickness of the internal boundary layer, δ_i can be represented by

$$\delta_i = 0.75 z_0 \left(\frac{x}{z_0} \right)^{0.8} \tag{10}$$

where x is the fetch length and z_0 is the roughness length. With this assumption, it follows that the fractional change in wind speed, $\Delta R = (U(x) - U_u)/U_u$ (where the subscript "u" refers to quantities at a point "upwind" of x) is given by (Taylor and Lee, 1984)

$$\Delta R = \begin{cases} 0 & \text{for } z \geq \delta_i \\ \dfrac{\ln(z/z_0)\ln(\delta_i/z_{0u})}{\ln(z/z_{0u})\ln(\delta_i/z_0)} - 1 & \text{for } z < \delta_i \end{cases} \tag{11}$$

where z is the reference measurement height. In the present case, U_u is taken as the wind speed at the shoreline and z_{0u} as the roughness length for the upwind land surface. Eq. (11) assumes that both the upwind boundary layer is logarithmic and that the developing internal boundary layer is logarithmic for $z < \delta_i$.

To apply this model requires estimates of both the upwind roughness, z_{0u} and the roughness at the fetch x, z_0. As mentioned above, the determination of the aerodynamic roughness of the finite depth wave roughened water surface still requires substantial research. In order to progress we have adopted the method proposed by Wu (1982). The surface roughness, z_0 can be obtained from the Charnock relationship (Charnock, 1955)

$$z_0 = a u_*^2 / g \tag{12}$$

with the Charnock "constant", $a = 0.0185$ (Wu, 1982). The friction velocity, u_* can be determined from the 10 m drag coefficient, C_{10} as (Wu, 1982)

$$u_*^2 = C_{10} U_{10}^2 \tag{13}$$

$$C_{10} = (0.8 + 0.065 U_{10}) \times 10^{-3} \tag{14}$$

This model was calibrated against the recorded wind profiles along the lake by determining optimal (in a least squares sense) values of z_{0u}. This analysis yielded $z_{0u} = 0.5$ m for northerly winds and $z_{0u} = 0.1$ m for southerly winds. The northern end of the lake consists of a lightly treed eucalyptus forest and the southern end is open grassland with occasional trees. The derived values of z_{0u} are typical of the values which could be expected for such surface conditions (Taylor and Lee, 1984). Fig. 5 shows a comparison between this model and the measured data. Within the measurement uncertainty of the data, the model agrees well with the data.

This observed variation of wind speed with fetch is not a peculiarity of the present experiment but a natural feature of fetch limited growth. With the exception of the work of Dobson et al. (1989) it has been neglected in all previous studies. Following Dobson et al. (1989) we adopt the 10 m wind speed averaged over the "down wind" fetch, $\overline{U}_{10}$ as the appropriate wind speed scaling parameter

$$\overline{U}_{10} = \frac{1}{x}\int_0^x U_{10}(x)\mathrm{d}x \tag{15}$$

In practice, since data was not always available at all the anemometer sites along the fetch, the continuous record at Station 6 has been utilized in all subsequent analysis, $\overline{U}_{10}$ being determined from these data by the application of Eq. (10) to Eq. (15).

6.2. Fetch

As indicated above, the north/south data set is limited to events for which the wind direction is within 20° of the alignment of the instrument array. This criterion has been introduced to avoid errors associated with slanting fetch conditions and to reduce any influence of the east/west boundaries of the lake (see Section 8). Hence the fetch has simply been determined as the distance along the array to the upwind shoreline. Account has however been taken of the variation in water level during the extended measurement period in determining the position of the shoreline. In addition, the down wind fetch averaged wind speed defined in Eq. (15) has been corrected to include only its component in the direction of the instrument array, $\overline{U}_{10}\cos\Delta\theta$ where $\Delta\theta$ is the angle between the wind direction and the line of the instrument array ($|\Delta\theta| < 20°$).

6.3. Water depth

Although the bathymetry of Lake George is extremely simple with a very uniform and flat bottom (see Fig. 1), there is some variation in water depth, particularly near the shore. To account for this variability, the water depth used in all subsequent analysis is the average depth along the upwind fetch, $\overline{d}$. In a similar manner to Eq. (15) this is defined as

$$\overline{d} = \frac{1}{x}\int_0^x d(x)\mathrm{d}x \tag{16}$$

The actual bathymetry of the lake as shown in Fig. 1 and used in Eq. (16) was obtained from a detailed hydrographic survey performed as part of the experiment.

In the remainder of this paper the "overbars" for $\overline{U}_{10}$ and $\overline{d}$ have been discarded for simplicity of presentation.

7. Asymptotic depth limit

Based on the limited Lake Okeechobe data set, Bretschneider (1958) proposed depth limitations to both ϵ and ν in terms of δ as reproduced in Eqs. (1) and (2). The rationale for the existence of such limits was explained in terms of the depth limited TMA

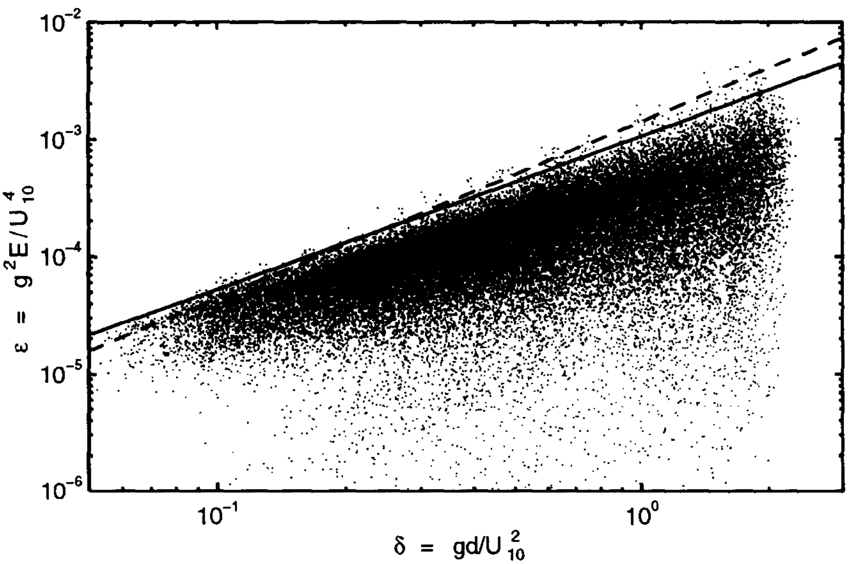

Fig. 6. A scatter plot of non-dimensional energy, ϵ against non-dimensional depth, δ. The full data set of approximately 65,000 points is shown. The envelope to the data is shown as the solid line (Eq. (17)) and the Lake Okeechobe result (Bretschneider, 1958) (Eq. (1)) as the dashed line.

spectral form (Bouws et al., 1985) by Vincent (1985) and Vincent and Hughes (1985). The approximate forms of Eqs. (1) and (2) were also confirmed by these studies.

The extensive data set from this experiment provides an ideal opportunity to refine these relationships. As the asymptotic depth limit is assumed to depend only on δ, the full data set can be utilized (result is independent of fetch). Fig. 6 shows a scatter plot of ϵ versus δ and Fig. 7 a scatter plot of ν versus δ. In both cases approximately 65,000 data points are shown. There appear to be clear depth defined limits for both ϵ and ν. Image enhancement techniques (edge detection) were used to rationally define these limits and power law forms fitted as envelopes to the data. These limits are given by

$$\epsilon = 1.06 \times 10^{-3}\delta^{1.3} \tag{17}$$

and

$$\nu = 0.20\delta^{-0.375} \tag{18}$$

Also shown in Fig. 6 and Fig. 7 are the lake Okeechobe results (Eqs. (1) and (2)) (Bretschneider, 1958). Eqs. (1) and (17) yield consistent results. Eq. (18), however, produces significantly larger values for ν than Eq. (2).

8. Fetch limited growth

Figs. 8 and 9 show scatter plots of ϵ (Fig. 8) and ν (Fig. 9) versus χ. The data have been partitioned into discrete intervals of δ. Individual ranges ofδ are shown in the

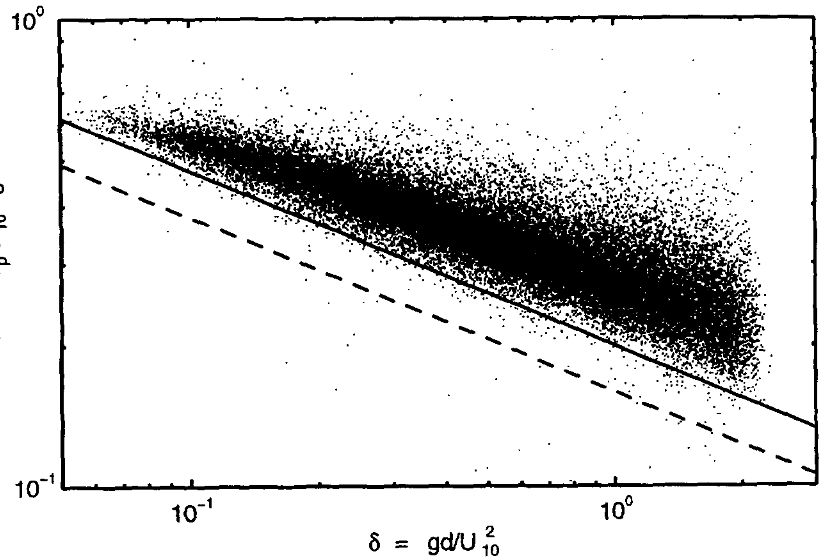

Fig. 7. A scatter plot of non-dimensional peak frequency, ν against non-dimensional depth, δ. The full data set of approximately 65,000 points is shown. The envelope to the data is shown as the solid line (Eq. (18)) and the Lake Okeechobe result (Bretschneider, 1958) (Eq. (2)) as the dashed line.

separate panels of Fig. 8 and Fig. 9. A preliminary investigation of the north/south data indicated that the data which conformed to deep water conditions were consistent with previous deep water growth law formulations. In particular, ϵ was well modelled by the JONSWAP relationship (Hasselmann et al., 1973), $\epsilon = 1.6 \times 10^{-7}\chi$ and ν by the result of Kahma and Calkoen (1992), $\nu = 2.18\chi^{-0.27}$.

Noting these deep water asymptotic limits to the data, together with the shallow water limits represented by Eqs. (17) and (18), generalized forms of Eqs. (3)–(8) are proposed to model the data.

$$\epsilon = 3.64 \times 10^{-3}\left\{\tanh A_1 \tanh\left[\frac{B_1}{\tanh A_1}\right]\right\}^n \tag{19}$$

where

$$A_1 = 0.292^{1/n}\delta^{1.3/n} \tag{20}$$

$$B_1 = \left(4.396 \times 10^{-5}\right)^{1/n}\chi^{1/n} \tag{21}$$

and

$$\nu = 0.133\left\{\tanh A_2 \tanh\left[\frac{B_2}{\tanh A_2}\right]\right\}^m \tag{22}$$

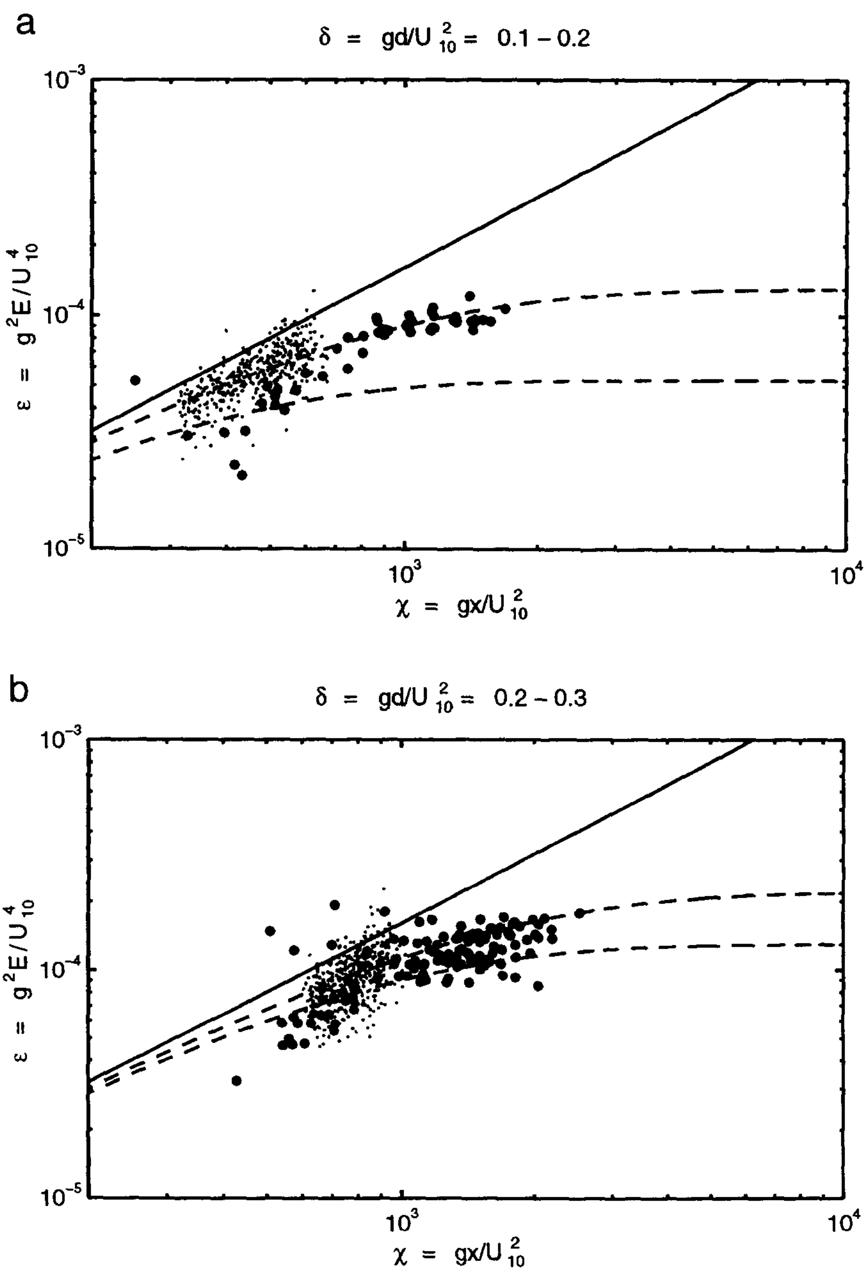
a
δ = gd/U²₁₀ = 0.1 – 0.2
10⁻³
10⁻⁴
10⁻⁵
ε = g²E/U⁴₁₀
10³
10⁴
χ = gx/U²₁₀
b
δ = gd/U²₁₀ = 0.2 – 0.3
10⁻³
10⁻⁴
10⁻⁵
ε = g²E/U⁴₁₀
10³
10⁴
χ = gx/U²₁₀

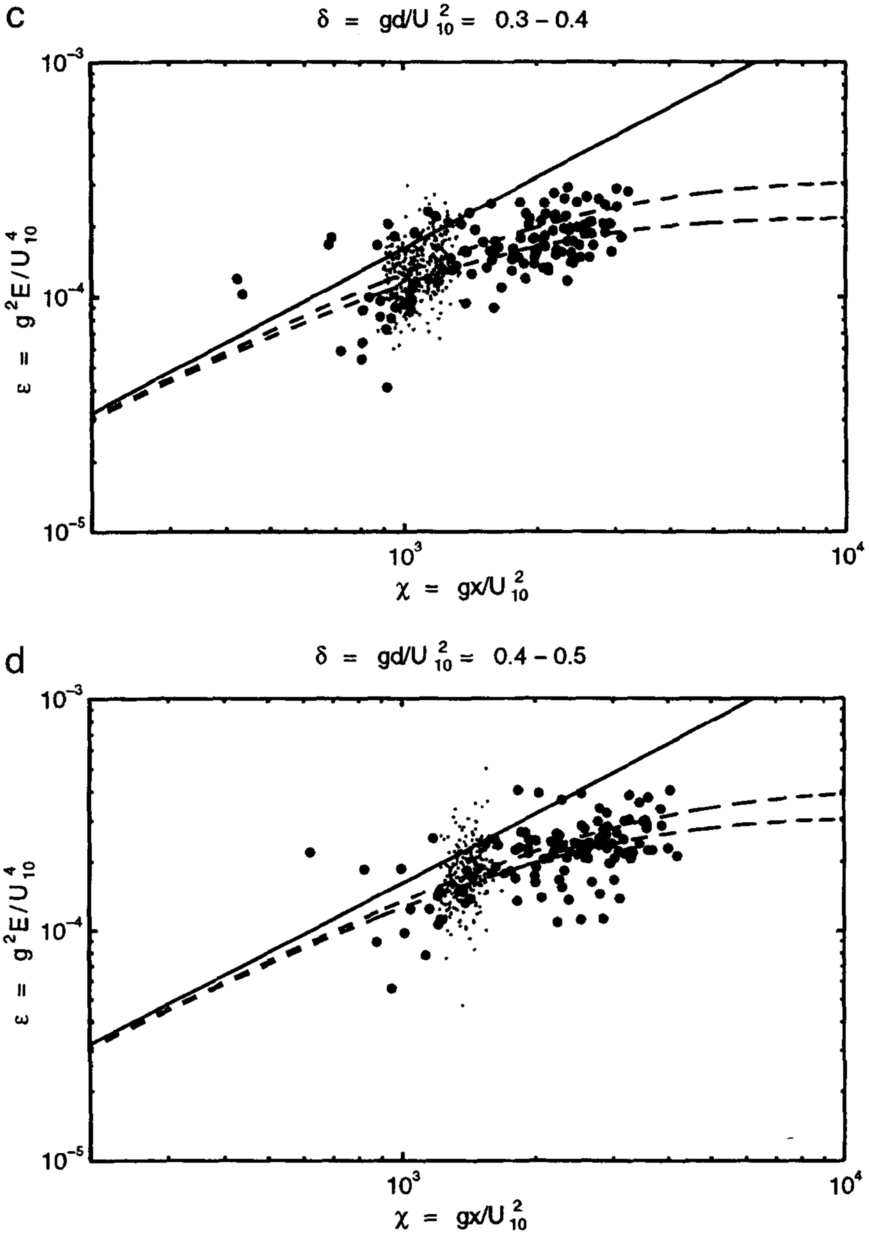

Fig. 8. (a) A scatter plot of non-dimensional energy, ϵ against non-dimensional fetch, χ. Only data with values of non-dimensional depth, δ between 0.1 and 0.2 are shown. The north/south data are shown as the large dots and the lower quality east/west data as the small dots. Eq. (25) is shown for the two extremes of δ (i.e. 0.1 and 0.2) by the two dashed lines. The deep water asymptotic form of Eq. (25) is shown as the solid line. (b) As (a) but for values of δ between 0.2 and 0.3. (c) As (a) but for values of δ between 0.3 and 0.4. (d) As (a) but for values of δ between 0.4 and 0.5.

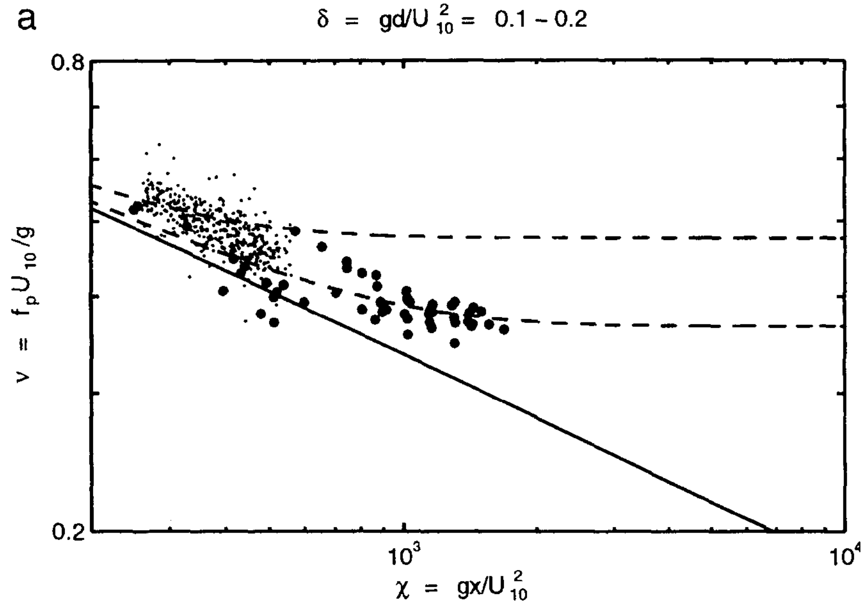

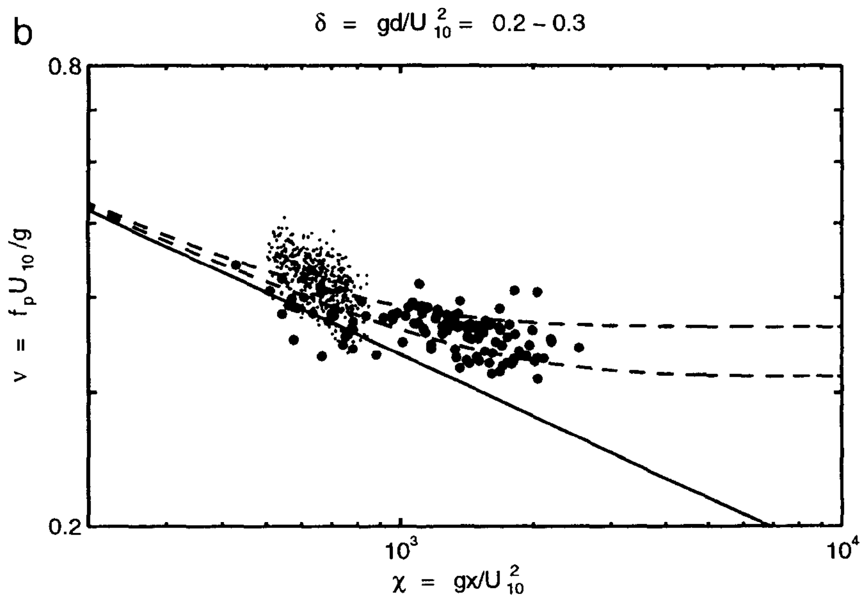

Fig. 9. (a) A scatter plot of non-dimensional peak frequency, ν against non-dimensional fetch, χ. Only data with values of non-dimensional depth, δ between 0.1 and 0.2 are shown. The north/south data are shown as the large dots and the lower quality east/west data as the small dots. Eq. (25) is shown for the two extremes of δ (i.e. 0.1 and 0.2) by the two dashed lines. The deep water asymptotic form of Eq. (25) is shown as the solid line. (b) As (a) but for values of δ between 0.2 and 0.3. (c) As (a) but for values of δ between 0.3 and 0.4. (d) As (a) but for values of δ between 0.4 and 0.5.

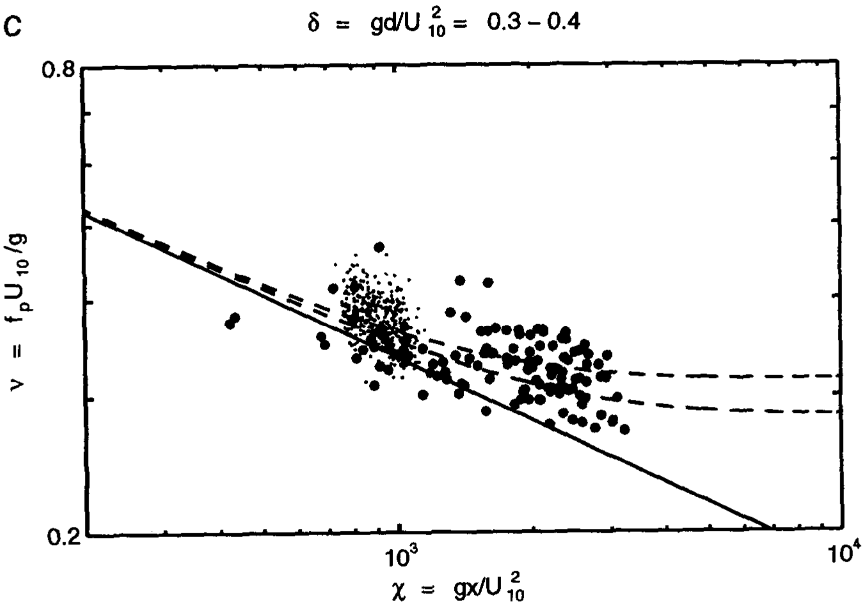

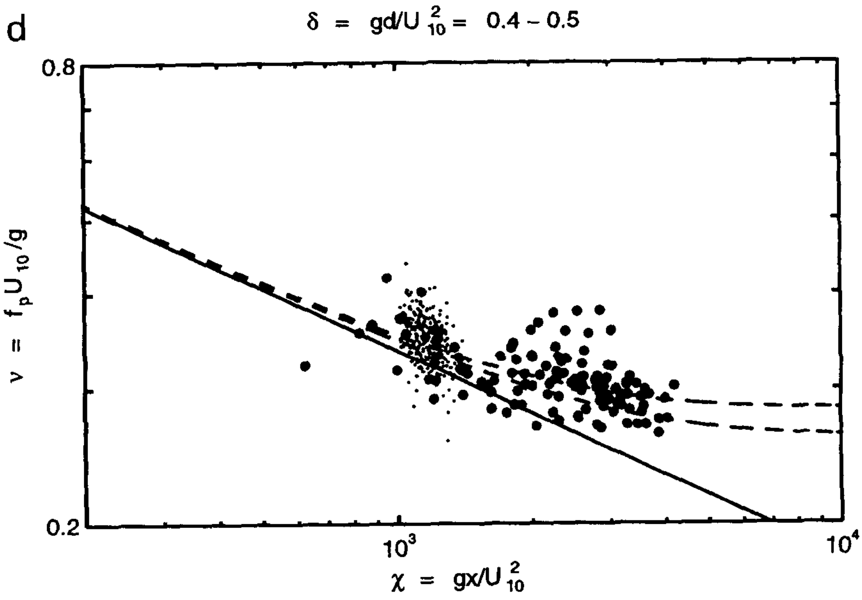

Fig. 9 (continued).

Table 3
Asymptotic limits of Eqs. (19) and (22)

	Eq. (19)	Eq. (22)
Deep water $\delta \to \infty$	$\epsilon = 1.6 \times 10^{-7}\chi$ Hasselmann et al. (1973)	$\nu = 2.18\chi^{-0.27}$ Kahma and Calkoen (1992)
Shallow water $\chi \to \infty$	$\epsilon = 1.06 \times 10^{-3}\delta^{1.3}$ Eq. (17)	$\nu = 0.20\delta^{-0.375}$ Eq. (18)
Long fetch Deep water $\chi \to \infty, \delta \to \infty$	$\epsilon = 3.64 \times 10^{-3}$ Pierson and Moskowitz (1964)	$\nu = 0.133$ Pierson and Moskowitz (1964)

where

$$A_2 = 1.505^{1/m}\delta^{-0.375/m} \tag{23}$$

$$B_2 = 16.391^{1/m}\,\chi^{-0.27/m} \tag{24}$$

The asymptotic limits of Eqs. (19)–(24) are independent of the choice of the exponents n and m, which control the rate of transition from "deep" to "depth limited" conditions. All asymptotic limits of the equations are summarized in Table 3.

A nonlinear least squares analysis was performed on the full north/south data set to determine n and m. This analysis yielded $n = 1.74$ and $m = -0.37$. Hence, Eqs. (19)–(24) reduce to

$$\epsilon = 3.64 \times 10^{-3}\left\{\tanh A_1 \tanh\left[\frac{B_1}{\tanh A_1}\right]\right\}^{1.74} \tag{25}$$

where

$$A_1 = 0.493\,\delta^{0.75} \tag{26}$$

$$B_1 = 3.13 \times 10^{-3}\chi^{0.57} \tag{27}$$

and

$$\nu = 0.133\left\{\tanh A_2 \tanh\left[\frac{B_2}{\tanh A_2}\right]\right\}^{-0.37} \tag{28}$$

where

$$A_2 = 0.331\,\delta^{1.01} \tag{29}$$

$$B_2 = 5.215 \times 10^{-4}\chi^{0.73} \tag{30}$$

Eqs. (25) and (28) are shown in Fig. 8 and Fig. 9 respectively. As each of the panels of these figures contains data for a finite range of δ (i.e. $\delta = 0.1–0.2$ in Fig. 8a),two curves are shown, one for each of the extremes of δ for that figure. As a range of values of δ is shown, data scatter is expected. The data should, however, lie between these two curves. Generally, the proposed relationships (Eqs. (25) and (28)) approximate the data well. As with all previous field measurements of this type there is some data scatter.

Section 9 presents a detailed error analysis which addresses this question. Also shown in Figs. 8 and 9 are the deep water asymptotic limits to Eqs. (25) and (28) as defined in Table 3.

At short non-dimensional fetch the waves are in deep water and approach the deep water asymptotic limits which are consistent with the numerous previous deep water data sets. As the non-dimensional fetch increases, the effects of the finite water depth become more pronounced and the data progressively deviate from the deep water limit. At relatively large values of non-dimensional fetch, further spectral development ceases as shown by the "plateau" regions of the curves in Figs. 8 and 9. Rather than there being a single universal growth curve, there are a family of curves, one for each value of non-dimensional depth. The "plateau" regions define the depth limitation to spectral development where ϵ and ν are completely defined by δ (i.e. the depth limits defined by Eqs. (17) and (18)).

Lake George is approximately twice as long as it is wide and whether this aspect ratio limits the wave development along the north/south fetch must be addressed. To investigate this point, cases for which the wind direction was approximately perpendicular to the long east and west boundaries of the lake were extracted from the full data set. As there are no measurements of wind speed along the fetch for these cases, only data from Station 6, where the wind was always measured have been considered. As these east/west events are common, we can be very selective with the data, retaining only those cases for which the wind direction is within $\pm 10°$ of normal to the respective shore lines. This east/west data set is also shown in Fig. 8 and Fig. 9. Since there is no detailed information to determine the development of the wind field with fetch for these cases and since there is moderately elevated land to the east and west of the lake (compared with north/south which is quite flat) the east/west data set is considered to be of inferior quality to the north/south data set. Nevertheless, the east/west data set is consistent with the north/south data, confirming that the lake geometry has no significant influence on the results. It should be noted that there is only a relatively small range of values of χ for each selected range of δ for the east/west data, since all data is obtained from only a single dimensional fetch of approximately 5 km. Also, since the east/west data is believed to be of lesser quality than the north/south data, it was not used in the nonlinear least squares curve fit used to develop Eqs. (25) and (28).

9. Error analysis

As with all previous field measurements of fetch limited growth, the results presented in Fig. 8 and Fig. 9 exhibit significant scatter. Indeed, since the finite depth nature of the present data set introduces an additional non-dimensional variable in δ, one could expect the data scatter to be larger than in comparable deep water experiments.

It is important to determine whether the extent of this scatter can be explained by statistical sampling variability and instrumental accuracy or whether it indicates a shortcoming in the analysis procedure. For instance, does it indicate the choice of an inappropriate scaling parameter in the definition of the non-dimensional variables (i.e. wind speed) or that there are additional variables that have been ignored in the analysis (i.e. boundary layer stability).

9.1. Monte Carlo error simulation methodology

An extensive Monte Carlo error analysis was performed to determine confidence limits for each data point in the north/south data set. Each of the measured quantities (U_{10}, x, E, f_p and d) which make up the non-dimensional quantities (δ, ϵ and ν) can be considered as statistical variables with a mean value (as used in the previous analysis) and some standard deviation. For each of the measured quantities, a specific probability distribution was assigned (details below) with a mean and other defining parameters obtained from the measurements. For each measurement, a total of 10,000 random realizations of the measured quantity, which conform to the specific probability distribution function, were generated. These realizations were then multiplied to form 10,000 randomly selected values of each non-dimensional quantity. Due to the nonlinear product constituting the non-dimensional quantities (e.g. U_{10}^2) they will follow some unknown probability distribution function. These values were then ranked in order of magnitude and the 2.5 and 97.5 percentile values selected to define the 95% confidence limits for the non-dimensional quantities.

9.1.1. Wind speed

The values of wind speed used in the non-dimensional quantities were determined as the means of the anemometer time series. Hence, not only the mean value, U_{10} but also the standard deviation, σ_u, is known. The quantity σ_u is the standard deviation of the 1 second values of u used to form U_{10}. Following Walpole and Myers (1972), the probability distribution function of the mean will follow a normal distribution, (irrespective of the probability distribution of the individual measurements comprising the mean) with a standard deviation, $\sigma_{U_{10}}$ given by

$$\sigma_{U_{10}} = \frac{\sqrt{\sigma_u^2}}{N} \tag{31}$$

where N is the number of points used to form the mean. Eq. (31) is true only if N is large. In the present context N was always of order 1000. Hence, the random realizations of U_{10} were generated so as to conform to a normal distribution with a mean of U_{10} and a standard deviation given by Eq. (31).

9.1.2. Fetch length

Even with the simplest of shore line geometries, there is some error in the estimation of the fetch, x. In addition, in the present context the actual position of the shoreline varied with the seasonal change in water depth. Measurements also indicated set-up and seiching could change the water level by approximately 10 cm. Although these quantities were all considered in determining the fetch, x, some error obviously results. The exact magnitude of this error is difficult to estimate. We have arbitrarily assumed that the error will follow a normal distribution with a standard deviation, $\sigma_x = 300$ m. This seems a realistic choice in view of the uncertainties described above. Due to the arbitrary nature of this estimate, no further effort has been made to include fetch length errors associated with the determination of the wind direction.

9.1.3. Total energy

The total energy, E was determined from the integral of the variance spectrum, $F(f)$ (i.e. $E = \int F(f)\mathrm{d}f$). Since $F(f)$ is determined from a finite time series, it has an associated sampling variability. Consequently, E will also have an associated sampling variability. Young (1986) has shown that the significant wave height, ($H_s = 4\sqrt{E}$) follows a chi-squared distribution with α degrees of freedom, χ^2_α where α is given by

$$\alpha = \frac{M\left[\int F(f)\mathrm{d}f\right]^2}{\int (F(f))^2 \mathrm{d}f} \tag{32}$$

where $M \approx 112$ is the number of degrees of freedom in the spectral estimate (see Section 4). Hence, individual realizations of H_s, from which E was calculated were generated to conform to this chi-squared distribution.

9.1.4. Peak frequency

Again, since f_p was determined from the spectrum, $F(f)$ (see Eq. (9)) it has an associated sampling variability. Young (1996) has shown that the resulting probability distribution depends on the spectral shape, the discrete frequency interval used in the spectrum (Δf) and the number of degrees of freedom in the spectral estimate, M. This approach has been adopted here for the generation of the random realizations of f_p.

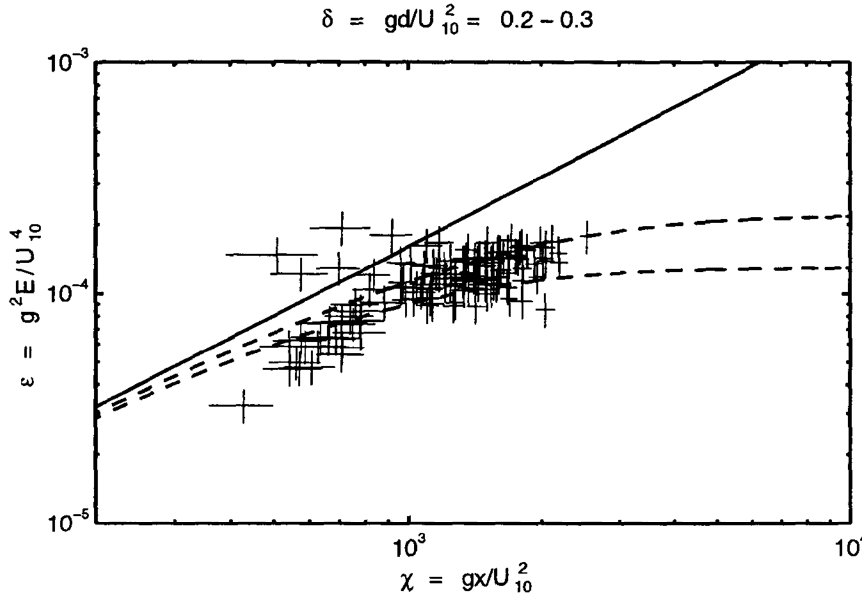

Fig. 10. A scatter plot of non-dimensional energy, ϵ against non-dimensional fetch, χ as in Fig. 8b. The 95% confidence limits on the data, as calculated from the Monte Carlo error analysis are included. Only the north/south data are considered.

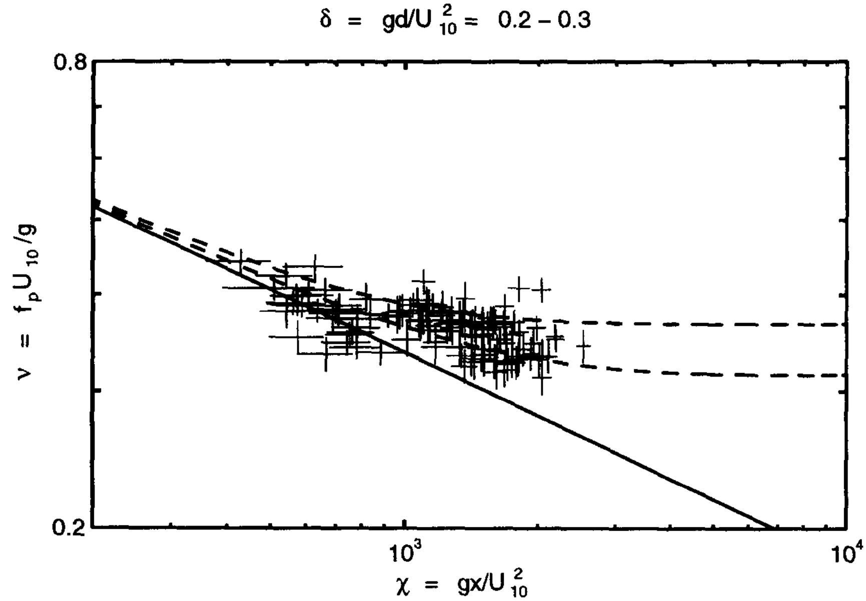

Fig. 11. A scatter plot of non-dimensional peak frequency, ν against non-dimensional fetch, χ as in Fig. 9b. The 95% confidence limits on the data, as calculated from the Monte Carlo error analysis are included. Only the north/south data are considered.

9.2. Monte Carlo simulation results

Fig. 10 and Fig. 11 reproduce the results shown in Fig. 8 and Fig. 9, but with the inclusion of error bars to show the magnitudes of the 95% confidence limits. The vast majority of the observed scatter in the results can be accounted for by the statistical sampling variability considered in this analysis. This is particularly so when the potential errors in determining δ are also considered. The results shown in Fig. 10 and Fig. 11 do not include the confidence limits for this third variable dimension.

The values of ϵ at short non-dimensional fetch do, however, appear abnormally low. This could possibly be due to an overestimation of the wind speed at short fetch. The deviation from the deep water curve shown in Fig. 10 is consistent with an overestimation of the wind speed by approximately 20%. As no anemometer was located at Station 1 (see Table 2), such a speculation cannot be substantiated. The results do, however, suggest that the wind speed profile predicted by Eq. (11) may be questionable in the early stages of the development of the lake boundary layer.

9.3. Spurious correlations

The wind speed appears in all of the non-dimensional parameters used in the growth analyses. Hence, it is possible for spurious correlations to develop between these quantities, simply due to errors in the common parameter (U_{10} in this case). This

Table 4
Possible spurious relationships between non-dimensional variables. Spurious relationships can occur due to errors in U_{10}, if the data comprising the multiplier (e.g. E/x^2 in first line) vary little in magnitude. The relationships found from the measured data are shown in column 2 and the ratio of the exponent in the spurious relationship to the exponent obtained from the measured data in column 3. The range of values from the data for the multiplier in column 1 are shown in column 4. If the Ratio of Exponents is near 1 and the Range of Multiplier is small, spurious correlations are possible

Spurious relationship	Experimental relationship	Ratio of exponents	Range multiplier
$\epsilon \equiv \frac{E}{x^2}\chi^2$	$\epsilon \propto \chi^{1.0} \to \chi^0$	$2.0 \to \infty$	$10^{-9} \to 10^{-11}$
$\nu \equiv f_p(\frac{x}{g})^{1/2}\chi^{-1/2}$	$\nu \propto \chi^{-0.27} \to \chi^0$	$1.9 \to \infty$	$8 \to 20$
$\epsilon \equiv \frac{E}{d^2}\delta^2$	$\epsilon \propto \delta^{1.3}$	1.5	$10^{-4} \to 10^{-2}$
$\nu \equiv f_p(\frac{d}{g})^{1/2}\delta^{-1/2}$	$\nu \propto \delta^{-0.375}$	1.3	$10^{-1} \to 10^0$

problem has been investigated in the context of deep water growth by Kahma and Calkoen (1992). Consider the relationship between ϵ and χ. The wind speed appears in ϵ to the power -4 and in χ to the power -2. Hence, a relationship of the form $\epsilon = (E/x^2)\chi^2$ represents a dimensionally correct spurious correlation. Provided the quantity E/x^2 was relatively constant and there were random errors in the values of U_{10}, an apparent correlation between ϵ and χ would exist. As a result, one must be skeptical of relations which are near these spurious correlations. Table 4 shows the derived spurious correlations for each of the variables discussed previously. These correlations are compared with the functional relationships found in Section 7 and Section 8.

For instance, the data indicates a relationship between ϵ and χ with an exponent which varies between 1.0 (deep water) and 0 (depth limited). This compares to the spurious correlation exponent of 2.0. Hence, the ratio of the exponents of the spurious correlation to the observed data are $2.0 \to \infty$. In addition, the spurious correlation multiplier, E/x^2 ranges over two orders of magnitude ($10^{-9} \to 10^{-11}$). As the ratio of the exponents is far from one and the multiplier is not constant, it is reasonable to conclude that the observed correlation is not spurious.

Similarly, examination of Table 4 shows that it can be confidently concluded that the correlations between ν–χ and ϵ–δ are also genuine. The validity of the relationship ν–δ is less easily assessed. The ratio of the exponents is only 1.3 although the multiplier does vary by an order of magnitude. We conclude that the correlation is genuine but with less confidence than for the other relationships.

10. Discussion and conclusions

The experiment described in this paper represents the first comprehensive attempt to measure the evolution of fetch limited waves in water of finite depth. Eqs. (25) and (28)

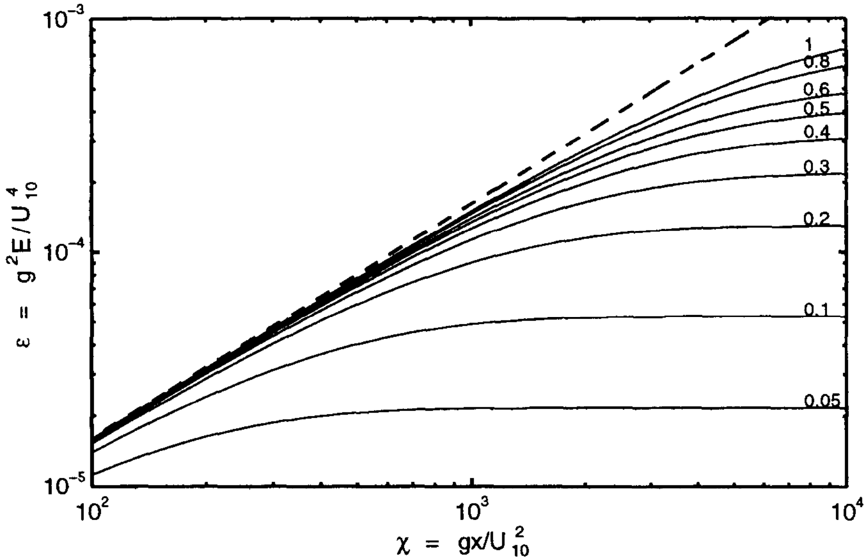

Fig. 12. The evolution of the non-dimensional energy, ϵ as a function of non-dimensional fetch, χ as predicted by Eq. (25). Each curve is for a specific value of non-dimensional depth, δ as shown at the right extremity of each curve.

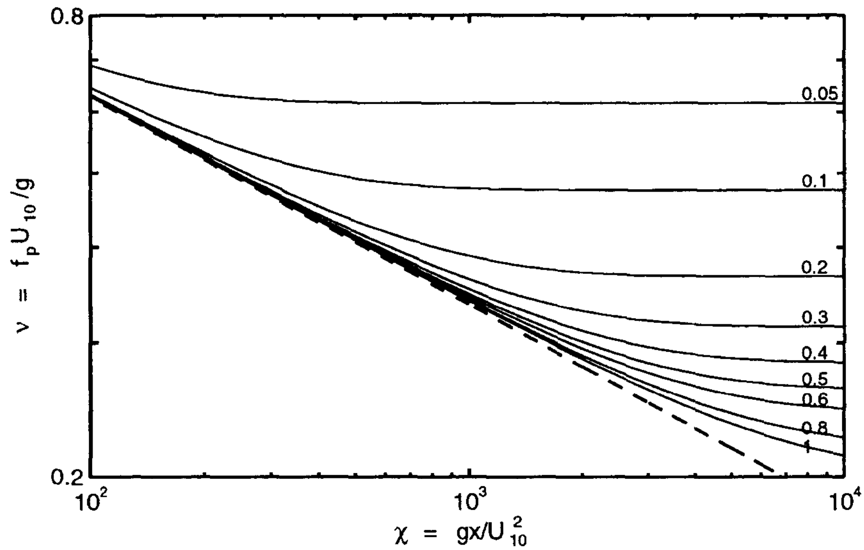

Fig. 13. The evolution of the non-dimensional peak frequency, ν as a function of non-dimensional fetch, χ as predicted by Eq. (28). Each curve is for a specific value of non-dimensional depth, δ as shown at the right extremity of each curve.

provide an acceptable mathematical (although empirical) summary of these data. These relationships are reproduced in graphical form in Fig. 12 and Fig. 13. Rather than finite depth fetch limited evolution being defined by a single power law as in deep water, a family of curves exist, one for each non-dimensional water depth, δ. At short non-dimensional fetch, the wave length is sufficiently short for waves to be in deep water and the relationships are comparable to those previously obtained for deep water. With increasing fetch, the effects of the finite depth become more pronounced. The total energy is smaller than would be expected in deep water and the peak frequency higher. With a further increase in fetch, a point is eventually reached where further spectral development ceases. At this point both the non-dimensional energy and peak frequency become depth limited.

The results presented above are valuable for engineering design and as a field data set for numerical model validation. In addition, however, they provide indirect insight into the processes responsible for the observed evolution. In an extension of the energy balance commonly used to describe the evolution of deep water spectra, the finite depth situation can reasonably be assumed to be a balance of the processes of: atmospheric input from the wind, S_{in}, nonlinear interactions within the spectrum, S_{nl}, dissipation due to "white-capping", S_{ds} and decay due to bottom friction, S_{bf}. Of these four terms, only bottom friction has been extensively investigated and, even here, mostly in the context of swell decay. The deep water formulation for atmospheric input is of the form $S_{in} \propto (u/C - 1)$ where u is a representative wind speed and C the phase speed. An extrapolation of this form to water of finite depth would suggest enhanced atmospheric input as C decreases with water depth. Similarly, the computations of Hasselmann and Hasselmann (1985) show that the magnitude of nonlinear interactions increases with decreasing water depth. Hence, one would conclude a more pronounced transfer of energy to lower frequencies than in deep water. White-cap dissipation is poorly understood in deep water and there has been no research into this process in finite depth conditions. It is reasonable to assume, however, that it may also be enhanced compared to deep water, as the steep wave conditions typical of finite depth conditions are accompanied by significant wave breaking. Thus it appears that all three of these source terms will be larger in finite depth conditions compared to comparable deep water cases. The fact that both S_{in} and S_{nl} should be more effective at transferring energy to low frequencies in finite depth conditions would tend to suggest that the peak frequency may be lower than in deep water for the same fetch. Exactly the opposite occurs, indicating that the dissipative processes of S_{ds} and S_{bf} are sufficiently large to counteract this effect.

It is well known that bottom friction is an important process when considering the propagation of swell into shallow coastal regions. Whether it is important in active fetch limited growth is difficult to assess. If all other source terms are significantly larger than in deep water, bottom friction may play only a minor role. Indeed, a comparison between the present results and the limited previous finite depth data suggests this may be the case. The depth limited growth relationship represented by Eq. (17) is very similar to the Lake Okeechobe form (Eq. (1)) (see also Fig. 6). It is also comparable with the form developed by Vincent and Hughes (1985). Additionally, Holthuijsen (1980) has presented a composite collection of results from largely unpublished sources which is again comparable to the present results. The depth limited asymptote occurs when all four source terms sum to yield zero at all spectral frequencies. If bottom friction is a significant term in this summation, a different result could be expected as the bed material, and hence the magnitude of S_{bf}, changes.

The bed material in Lake George is a relatively fine grained but cohesive mud. The bed is not mobile and ripples do not develop. Although not reported, it is reasonable to assume that Lake Okeechobe would be similar. The TMA data (Bouws et al., 1985) from which Vincent and Hughes (1985) developed their depth limited form comes from three separate coastal data sets where sand of varying grain diameter was the bed material. Similarly the Holthuijsen (1980) data is from a range of sites. The fact that these diverse data sets yield similar results tends to suggest that the effects of bottom friction (bottom dissipation) are relatively minor in these fetch limited conditions.

If this situation occurs at the depth limited asymptote, where bottom friction would be at its maximum, it is reasonable that a similar situation would also exist at shorter fetches. Under this assumption the present results should universally hold and differing bed materials would have only a minor influence on the observed growth curves.

The importance of these questions is obvious, particularly in the context of attempting to develop finite depth wave prediction models. The lack of direct measurements of the respective source terms in finite depth conditions is a clear deficiency in our collective knowledge. It is hoped the research community will be able to address these deficiencies in the near future.

Acknowledgements

Numerous members of the technical staff of the School of Civil Engineering, Univ. College, UNSW have made enormous contributions to the success of this large field experiment. Mary Dalton and Peter McMahon of our electronics section have designed and constructed all electronics used in the project, the reliability of the instrumentation speaks volumes for their skills. The support towers, central platform and numerous other components were constructed by John MacLeod, Doug Collier and Bernie Miller. In addition, numerous other members of staff have assisted in the deployment and maintenance of instruments. They include: Graham Johnston, Jon Delaney, Terry Lutze, David Sharp and Jim Baxter. The project could not have been successful without the significant contributions from this large and very skilled group of people. The project was funded by the Australian Research Council, without which it would have been impossible. This contribution is gratefully acknowledged.

References

Battjes, J.A., Zitman, T.J. and Holthuijsen, L.H., 1987. A reanalysis of the spectra observed in JONSWAP. J. Phys. Oceanogr., 17: 1288–1295.

Bouws, E., 1986. Provisional results of a wind wave experiment in a shallow lake (Lake Marken, The Netherlands). KNMI Afdeling Oceanografisch Onderzoek, OO-86-21, De Bilt, 15 pp.

Bouws, E., Günther, H., Rosenthal, W. and Vincent, C.L., 1985. Similarity of the wind wave spectrum in finite depth water, 1. Spectral form. J. Geophys. Res., 90: 975–986.

Bretschneider, C.L., 1958. Revised wave forecasting relationships. In: Proc. 6th Conference on Coastal Engineering, Gainesville/Palm Beach/Miami Beach, FL. ASCE, New York, pp. 30–67.

Bretschneider, C.L. and Reid, R.O., 1953. Change in wave height due to bottom friction, percolation and refraction. In: 34th Annual Meeting of American Geophysical Union.

CERC, 1977. Shore Protection Manual. U.S. Army Coastal Engineering Research Center. 3 Volumes.

CERC, 1984. Shore Protection Manual. U.S. Army Coastal Engineering Research Center. 2 Volumes.

Charnock, H., 1955. Wind stress on a water surface. Q. J. R. Meteorol. Soc., 81: 639–640.

Dobson, F., Perrie, W. and Toulany, B., 1989. On the deep-water fetch laws for wind-generated surface gravity waves. Atmos.-Ocean, 27: 210–236.

Donelan, M.A. and Pierson, W.J., 1987. Radar scattering and equilibrium ranges in wind-generated waves with application to scatterometry. J. Geophys. Res., 92: 4971–5029.

Donelan, M.A., Hamilton, J. and Hui, W.H., 1985. Directional spectra of wind-generated waves. Philos. Trans. R. Soc. London, A315: 509–562.

Donelan, M., Skafel, M., Graber, H., Liu, P., Schwab, D. and Venkatesh, S., 1992. On the growth rate of wind-generated waves. Atmos.-Ocean, 30: 457–478.

Ebuchi, N., Kawamura, H. and Toba, Y., 1992. Growth of wind waves with fetch observed by the Geosat altimeter in the Japan Sea under winter monsoon. J. Geophys. Res., 97: 809–819.

Hasselmann, K. et al., 1973. Measurements of wind-wave growth and swell decay during the Joint North Sea Wave Project (JONSWAP). Dtsch. Hydrogr. Z. Suppl. A, 8(12), 95 pp.

Hasselmann, S. and Hasselmann, K., 1985. Computations and parameterizations of the nonlinear energy transfer in a gravity-wave spectrum. Part 1: A new method for efficient computations of the exact nonlinear transfer integral. J. Phys. Oceanogr., 15: 1369–1377.

Holthuijsen, L.H., 1980. Methoden voor golfvoorspelling. Technische Adviescommissie voor de Waterkeringen, Netherlands.

Ijima, T. and Tang, F.L.W., 1966. Numerical calculations of wind waves in shallow water. In: Proc. 10th Conf. on Coastal Eng., Tokyo. ASCE, New York, Vol. 2, pp. 38–45.

Janssen, P.A.E.M., 1989. Wave-induced stress and the drag of airflow over sea waves. J. Phys. Oceanogr., 19: 745–754.

Kahma, K.K., 1981. A study of the growth of the wave spectrum with fetch. J. Phys. Oceanogr., 11: 1503–1515.

Kahma, K.K. and Calkoen, C.J., 1992. Reconciling discrepancies in the observed growth of wind-generated waves. J. Phys. Oceanogr., 22: 1389–1405.

Kitaigorodskii, S.A., 1962. Applications of the theory of similarity to the analysis of wind-generated wave motion as a stochastic process. Izv. Akad. Nauk SSSR Geophys. Ser., 1: 105–117.

Pierson, W.J. and Moskowitz, L., 1964. A proposed spectral form for fully developed wind seas based on the similarity theory of S.A. Kitaigorodskii. J. Geophys. Res., 69(24): 5181–5190.

Smith, P.C. and MacPherson, J.I., 1987. Cross-shore variations of near-surface wind velocity and atmospheric turbulence at the land–sea boundary during CASP. Atmos.-Ocean, 25: 279–303.

Smith, S.D. et al., 1992. Sea surface wind stress and drag coefficients: The HEXOS results. Boundary-Layer Meteorol., 60: 109–142.

Taylor, P.A. and Lee, R.J., 1984. Simple guidelines for estimating wind speed variations due to small-scale topographic features. Climatol. Bull., 18: 3–32.

Thijsse, J.Th., 1949. Dimensions of wind-generated waves. In: General Assembly of Association d'Océanographie Physique, Oslo. Procés-Verbaux No. 4, pp. 80–81.

U.S. Army Corps of Engineers, 1955. Waves and wind tides in shallow lakes and reservoirs. Summary Report, Project CW-167, Jacksonville District, FL.

Vincent, C.L., 1985. Depth-controlled wave height. ASCE J. Waterw. Port Coastal Ocean Eng., 111: 459–475.

Vincent, C.L. and Hughes, S.A., 1985. Wind wave growth in shallow water. ASCE J. Waterway Port Coastal Ocean Eng., 111: 765–770.

Walpole, R.E. and Myers, R.H., 1972. Probability and Statistics for Engineers and Scientists. Macmillan, New York, 506 pp.

Walsh, E.J., Hancock, D.W. and Hines, D.E., 1989. An observation of the directional wave spectrum evolution from shoreline to fully developed. J. Phys. Oceanogr., 19: 670–690.

Wu, J., 1982. Wind-stress coefficients over sea surface from breeze to hurricane. J. Geophys. Res., 87: 9704–9706.

Young, I.R., 1986. Probability distribution of spectral integrals. ASCE J. Waterw. Port Coastal Ocean Eng., 112: 338–341.

Young, I.R., 1996. The determination of confidence limits associated with estimates of the spectral peak frequency. Ocean Eng., in press.

Young, I.R. and Van Vledder, G.Ph., 1993. A review of the central role of nonlinear interactions in wind-wave evolution. Philos. Trans. R. Soc., 342: 505–524.

Young, I.R., Verhagen, L.A. and Banner, M.L., 1995. A note on the bi-modal directional spreading of fetch-limited wind waves. J. Geophys. Res., 100: 773–778.

Zwarts, C.M.G., 1974. Transmission line wave height transducer. In: Int. Symp. on Wave Measurement and Analysis, pp. 605–620.